Available online at www.sciencedirect.com
ScienceDirect
Journal of Power Sources 177 (2008) 426–433
JOURNAL OF POWER SOURCES
www.elsevier.com/locate/jpowsour

Comparison of heat and mass transfer between planar and MOLB-type SOFCs

Yunzhen Yang [a], Guilan Wang [a], Haiou Zhang [b,*], Weisheng Xia [a]

[a] State Key Laboratory of Material Processing and Die & Mould Technology, Huazhong University of Science & Technology, Luoyu, Wuhan 430074, PR China

[b] State Key Laboratory of Digital Manufacturing and Equipment Technology, Huazhong University of Science & Technology, Wuhan 430074, PR China

Received 9 August 2007; received in revised form 23 October 2007; accepted 5 November 2007
Available online 19 November 2007

Abstract

A numerical simulation tool for calculating the planar and mono-block layer built (MOLB) type solid oxide fuel cells (SOFC) is described. The tool combines the commercial computational fluid dynamics simulation code with an electrochemical calculation subroutine. Its function is to simulate the heat and mass transfer and to predict the temperature distribution and mass fraction of gaseous species in the SOFC system. The three-dimensional geometry model of SOFC was designed to simulate a co-flow case and counter-flow case. The finite volume method was employed to calculate the conservation equations of mass, momentum and energy. Moreover, the influences of working conditions on the performances of planar and MOLB-type SOFCs were also discussed and compared, such as the delivery rate of gas and the components of fuel gas. Simulation results show that the MOLB-type SOFC has higher fuel utilization than the planar SOFC. For the co-flow case, average temperatures of PEN (positive electrode–electrolyte–negative electrode) in both types of SOFCs rise with the increase in delivery rate and mass fraction of hydrogen. In particular, the temperature of planar SOFC is more sensitive to the working conditions. In order to decrease the average temperatures in SOFC, it is effective to increase the delivery rate of air.

Keywords: Planar SOFC; MOLB-type SOFC; Thermo-electrochemical model; Temperature distribution; Gas mass fraction distribution

1. Introduction

Solid oxide fuel cell has been looked as a promising alternative energy source for residential and distributed power plants because of its higher energy conversion efficiency and power density, low environmental hazards and potentially low production cost. Thus, SOFC is expected to realize commercialization within a few years [1–3]. However, the further development of the SOFC has the challenges related to maximize the power density and minimize the non-uniform temperature distribution, which contributed to the thermal stress in the SOFC components [4,5], so the heat and mass transfer in the SOFC need to be researched.

The heat and mass transfer in the SOFC are influenced not only by geometrical designs of SOFC but also by the working conditions. In the past, some researchers have performed on preparing the electrode and electrolyte materials [6–9] and designing geometry of SOFC [10–13]. Thereinto, the planar SOFC has received much more attention than the tubular SOFC because of its easier fabrication and higher power density. In recent years, another type SOFC, which was MOLB-type SOFC, has also been researched. Such design has been in favor of enhancing its mechanical strength and the corrugate-shaped PEN provides the film with the combined function of fuel and air-flow paths, so the cell stacks are more compact and the laborious work of channel machining is less.

Besides the geometrical designs, the working conditions, such as delivery rates and hydrogen mass fraction of fuel and air to the cell system also influence on the performances of SOFC in a complex way. Thus, in order to efficiently develop SOFC stacks, it is convenient and effective to have the capability to experiment numerically with the effects of

* Corresponding author. Tel.: +86 27 87543493.
E-mail addresses: yyzhenhust@hotmail.com (Y. Yang), zholab@mail.hust.edu.cn (H. Zhang).

0378-7753/$ – see front matter © 2007 Elsevier B.V. All rights reserved.
doi:10.1016/j.jpowsour.2007.11.025

geometric designs and operation conditions on SOFC performances. In the past, modeling of the SOFC during steady operation has been constructed to calculate temperature distribution [14–20]. Investigations of planar and MOLB-type SOFCs operation and performance have predicted cell temperature distributions for various flow patterns [21–24]. However, only a little work has been performed on the influences of the operating conditions on the performances of planar SOFC [25,26], or even saying nothing of the influences on the MOLB-type SOFC.

The objective of present work is to compare the heat and mass transfer in the conventional planar with that in the MOLB-type SOFC. A CFD model tool is demonstrated to predict temperature distributions and gas species distributions of two-design SOFCs system. The results simulated in this paper can not only guide the designer in understanding how geometrical design affects the thermodynamics performances in the SOFC, but also provide a more reasonable basis for geometrical design of the SOFC stacks.

2. Mathematics model

2.1. Model geometry

Fig. 1(a) schematically shows a typical planar SOFC. PEN plate is sandwiched between the inter-connectors, which are machined with passages for channeling the fuel and air to the fuel cell. Fig. 1(b) demonstrates the MOLB-type SOFC and the PEN is modeled into a corrugated shape [21]. The fuel and air flow in the trapezoidal channels are separated by the corrugated PEN. For sake of simplicity in the calculation, one repeating cell unit was analyzed in this simulation (as shown in Fig. 1). In this model, for the two-design SOFCs, the thicknesses of anode, cathode, electrolyte and inter-connector were 0.5, 0.25, 0.05 and 1.0 mm, respectively.

2.2. Thermo-fluid model

The ANSYS-CFX code was selected to solve the thermo-fluid model. In the simulation, the conservation equations of species, mass, momentum and energy were solved using the finite volume method.

In general, gas species transfer mainly by convection in the flow channels and diffusion in the porous electrodes. The species conservation equation:

$$\nabla(\rho C_k U) = \nabla(D_{k,\text{eff}} \nabla C_k) + I_k, \quad k = \text{H}_2, \text{O}_2, \text{H}_2\text{O} \tag{1}$$

where I_k is the rate of production or consumption of species k, and given by [27]:

$$I_k = \pm \frac{s_k i}{2F} \tag{2}$$

where s_k is the chemical computation coefficients, i is the local current density, and F is the Faraday constant.

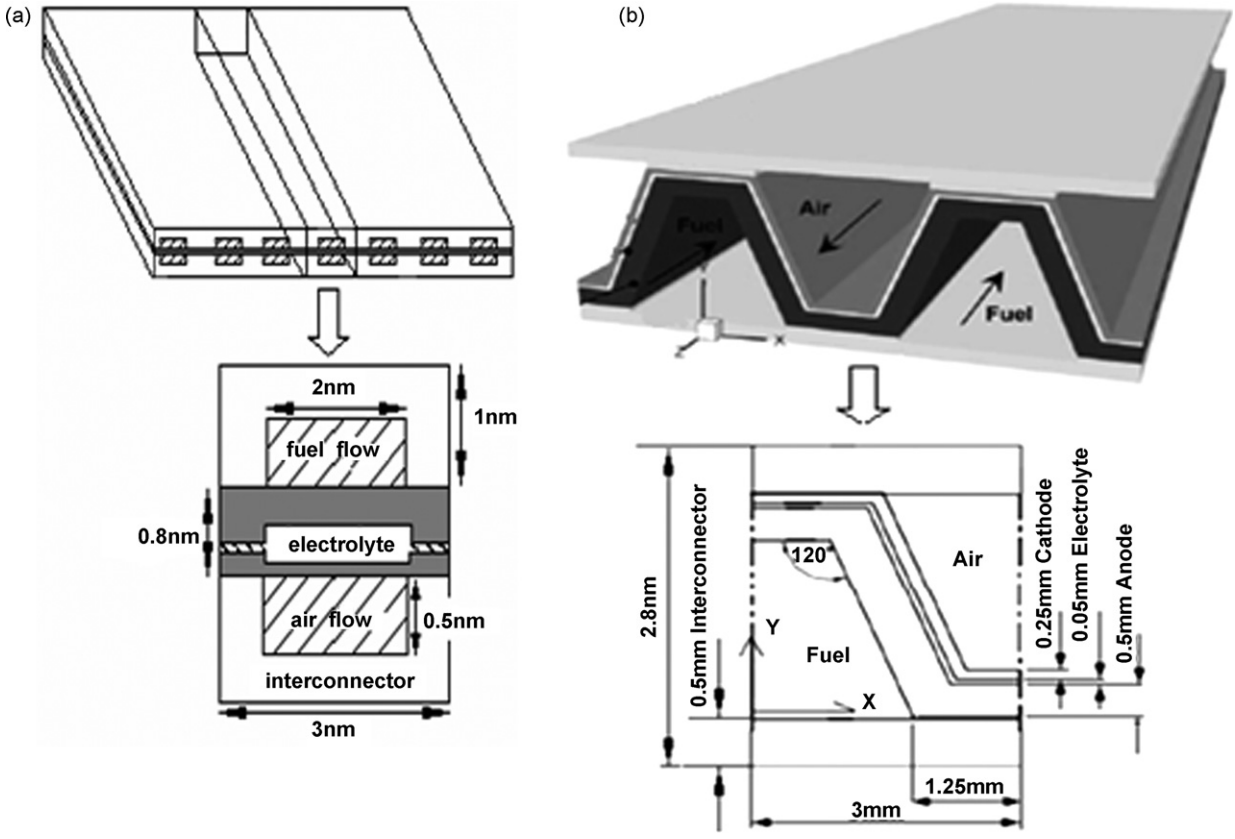

Fig. 1. Illustrations of the one cell-stack and the single unit model for planar SOFC (a) and MOLB-type SOFC (b).

The diffusion coefficient of gas is obtained by [28]:

$$D_{H_2} = 0.753 \times 10e-4 \times \left(\frac{T}{273}\right)^{1.5},$$

$$D_{O_2} = 0.181 \times 10e-4 \times \left(\frac{T}{273}\right)^{1.5} \quad (3)$$

where D_{H_2} and D_{O_2} are the diffusivity of H_2 and O_2, respectively, unit is $m^2\ s^{-1}$.

Although the mass is added on the anode and removed on the cathode, but the decrement of mass on the cathode is equal to increment of mass on the anode, so the mass in the whole SOFC system is conservational. The mass conservation equation:

$$\nabla(\varepsilon\rho U) = 0 \quad (4)$$

Both the air and fuel flows were considered as ideal gas mixtures with the density given by

$$\rho = \frac{P}{RT}\left(\sum_k \frac{m_k}{M_k}\right) \quad (5)$$

where m_k is the mass fraction of species k with molecular weight M_k and R is the gas constant.

The momentum conservation equation:

$$\rho\varepsilon\left(u\frac{\partial u}{\partial x} + v\frac{\partial v}{\partial y} + w\frac{\partial w}{\partial z}\right) = -\varepsilon\nabla P + \varepsilon\mu_{\text{eff}}\left(\frac{\partial u^2}{\partial x^2} + \frac{\partial v^2}{\partial y^2} + \frac{\partial w^2}{\partial z^2}\right) + S_M \quad (6)$$

where ε is the porosity of electrode, P is the pressure, μ_{eff} is the effective viscosity of the mixture gas and is given by [27]:

$$\mu_{\text{eff}} = \sum_k \frac{X_k\mu_k}{\sum_k X_k\phi_{kj}} \quad (7)$$

$$\phi_{kl} = \frac{\left[1 + (\mu_k/\mu_j)^{1/2}(M_j/M_k)^{1/4}\right]^2}{\left[8(1 + M_k/M_j)\right]^{1/2}} \quad (8)$$

In Eq. (6), S_M is momentum source and $S_M = 0$ in the flow channels. However, in the porous electrodes, Darcy law with constant porosity and permeability is applied to model the momentum source as follows [25]:

$$S_M = -\frac{\mu_{\text{eff}}}{K}\varepsilon^2 U \quad (9)$$

where X_k is the molar percent of the species k, μ_j, and μ_k are kinematical viscosities of species j and k, respectively.

Table 1
Coefficients of the specific heats of gas

Gas	a	b	c
Hydrogen	25.8911	−0.8373	2.0138
Oxide	29.0856	12.9874	−3.8644
Water gas	30.3794	9.6212	1.1848

Heat transfer between the fluid and solid materials was limited to conduction and convection, and radiation was neglected in this calculation because it is very small relative to the other kinds of heat transfer mechanisms. So the energy conservation equation is:

$$\nabla(U(\rho E_f + p)) + \nabla(\tau U) + \nabla(k_{\text{eff}}\nabla T) + S_E = 0 \quad (10)$$

where ρ is the density of the gas fluid, E_f is the total fluid energy, τ is the stress tensor, and k_{eff} is the effective thermal conductivities of porous electrodes, which are calculated as follows [29]:

$$k_{\text{eff}} = \varepsilon k_f + (1 - \varepsilon)k_s \quad (11)$$

where k_f and k_s are thermal conductivities of fluid and solid, respectively. S_E is energy source expressed by Eq. (12) and mainly consists of reaction and Ohmic heats [27].

$$S_E = \frac{i^2}{\sigma_{\text{eff}}} + \frac{i}{\delta}\left(\frac{T\Delta S}{2F} + \eta_{\text{act}}\right) \quad (12)$$

where i is the local current density, σ_{eff} is the effective electrical conductivity, δ is the anode thickness, ΔS is the change of entropy in the reaction and η_{act} is the activation potential.

Temperature-dependent specific heat of gas is used in the simulation, which are as follows [27]:

$$C_p = a + b \times 10^3 T + c \times 10^6 T^2 \quad (13)$$

where a, b, and c are relevant coefficients, as listed in Table 1. Solid material properties used in this simulation are listed in Table 2.

2.3. Electrochemical model

2.3.1. Assumptions and reactions

The oxidant reduction reaction occurring at the cathode is expressed as follows:

$$0.5\,O_2 + 2e^- \rightarrow O^{2-} \quad (14)$$

Table 2
Properties of the solid materials

Cell component	Density (kg m^{-3})	Effect thermal conductivity (W (m K)$^{-1}$)	Specific heat (J (kg K)$^{-1}$)	Porosity (%)	Permeability coefficient (m^2)
Interconnect	7700	13	0.8	–	–
Anode	6200	6.23	0.65	35	1.0E-12
Cathode	6000	9.6	0.9	35	1.0E-12
Electrolyte	5560	2.7	0.3	–	–

The oxygen ions transfer through the electrolyte and then into the active reaction areas of anode. The electrochemical reaction of fuel at the anode is

$$H_2 + O^{2-} \rightarrow H_2O + 2e^- \quad (15)$$

So the overall reaction is

$$H_2 + \tfrac{1}{2}O_2 \rightarrow H_2O \quad (16)$$

2.3.2. Dynamics of electrochemical reactions

According to the Faraday law, the reaction rates depend on the current density i [15]:

$$i = 2F\frac{df}{dt} = 4F\frac{dO_2}{dt} \quad (17)$$

where df/dt and dO_2/dt are the molar consumption rates of fuel and oxygen at the anode and the cathode, respectively.

During the process of energy transforming, when the charge transfer reaction at the electrolyte–electrode interface is too slow to provide ions at the rate required by the demand of current, the activation polarization occurs and is defined by the Butler–Volmer equation [30]:

$$i = i_0\left\{\exp\left(-\beta\frac{2F}{RT}\eta_{act}\right) - \left[\exp(1-\beta)\frac{2F}{RT}\eta_{act}\right]\right\} \quad (18)$$

Eq. (18) is simplified and described by the empirical formula and Tafel equation in anode and cathode, respectively [29,30]:

$$\eta_{act,a} = \frac{RT}{2Fi_{0,a}}i \quad (19)$$

$$\eta_{act,c} = -\left(\frac{RT}{2\beta F}\right)\ln i_{0,c} + \left(\frac{RT}{2\beta F}\right)\ln i \quad (20)$$

where β is the transmission coefficient and $\beta = 0.5$ in this simulation, $\eta_{act,a}$ and $\eta_{act,c}$ are the activation potentials at the anode and the cathode, respectively. $i_{0,a}$ and $i_{0,c}$ are the exchange current densities at the anode and the cathode, respectively.

Theoretical voltage of cell is obtained by the Nernst equation:

$$E = E_0 + \frac{RT}{2F}\ln\left(\frac{p_{H_2O}}{p_{H_2}\times p_{O_2}^{0.5}}\right) = \frac{RT}{2F}\ln K + RT\times\ln\left(\frac{p_{H_2}\times p_{O_2}^{0.5}}{p_{H_2O}}\right) \quad (21)$$

where K is the equilibrium constant of reaction under the standard atmosphere, E_0 is the standard voltage of the cell, p_{H_2O}, p_{O_2}, and p_{H_2} are the partial pressures of water gas, oxygen and hydrogen, respectively.

3. Numerical implementation

In the calculations, the modeling tool couples an electrochemical calculation method with a commercial computational fluid dynamics (CFD) simulation code. The finite volume Navier–Stokes and transport equations are solved to obtain the gas species mass fraction and temperatures at each position in the cell. The information is passed to the electrochemical model (subroutine). Then the local current density is calculated and applied to obtain the hydrogen reaction rate, heat source and species sources. Gas species mass fraction and temperature distributions are then calculated for the next iteration, and so on, until convergence of solution is achieved.

4. Simulation results and discussion

The cell voltage imposed on both geometries is 0.3 V. In the porous electrodes, typical values are employed for porosity of both electrodes $\varepsilon = 0.5$, tortuosity of anode is 4.5, tortuosity of cathode is 3, and permeability is $1.7\times10^{-10}\,m^2$. In this study, exchange current densities at the anode and the cathode are $5300\,A\,m^{-2}$ and $2300\,A\,m^{-2}$, respectively. And other cell operating conditions, including the delivery rate of fuel and hydrogen mass fraction in the fuel inlet are listed in Table 3.

Fig. 2 compares the PEN temperature distributions between planar SOFC and the MOLB-type SOFC for co-flow case (no. 1).

Table 3
The cell operating conditions and parameters used for simulation

Sample number case	Fuel			Air		Flow pattern
	Delivery rate (v1) ($m\,s^{-1}$)	Inlet temperature (K)	Hydrogen mass fraction (%)	Delivery rate (v2) ($m\,s^{-1}$)	Inlet temperature (K)	
1	0.5	973	0.8	3	873	Counter-flow
2						Co-flow
3	0.5 1.0 1.5	973	0.8	3	873	Co-flow
4	0.5	973	0.8 0.9 1	3	873	Co-flow
5	0.5	973	0.8	3 2 1	873	Co-flow

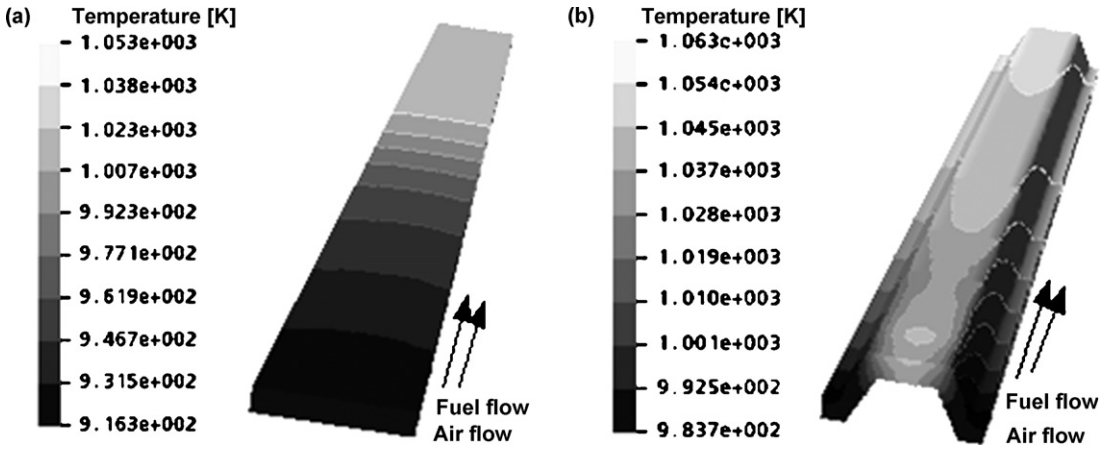

Fig. 2. PEN temperature distributions for planar SOFC (a) and MOLB-type SOFC (b) in the co-flow case (no. 1).

Although the structure of SOFC between these two geometries is different, the general trends in the temperature distributions are similar in essential. It is briefly described as follows. The average PEN temperature in planar SOFC is 979 °C with maximum and minimum temperatures of 1053 °C and 916 °C, respectively. Moreover, the PEN average temperature is 1014 °C with maximum and minimum temperatures of 1063 °C and 987 °C in MOLB-type SOFC. Thereby, the average temperature is higher and the temperature difference (ΔT) is lower in MOLB-type SOFC. This is because the electrochemical reaction active area of MOLB-type SOFC is larger than that of planar SOFC, so more gas is consumed in the active areas, as a result, more reaction heat is accumulated and the average temperature is higher.

Fig. 3 compares the PEN hydrogen mass fraction distributions between planar SOFC and the MOLB-type SOFC for co-flow case (no. 1). The hydrogen mass fraction for both types of SOFCs decrease along the fuel flow direction, but the difference of hydrogen mass fraction in the fuel inlet and outlet is lower in MOLB-type SOFC (Fig. 3(b)) than that in planar SOFC (Fig. 3(a)), So more hydrogen is consumed because the hydrogen mass fraction in the fuel inlet is same, which means that the fuel utilization is higher in the MOLB-type SOFC. In particular, due to the corner effect formed by the inclined plane and the upper plane, the temperature and hydrogen mass fraction distributions in MOLB-type SOFC are less uniform than those in planar SOFC.

Fig. 4 compares the temperature distributions of the two types of SOFCs in the counter-flow case (no.2), the average temperature is 996 °C with maximum and minimum temperatures of 1088 °C and 923 °C in planar SOFC, and the PEN average temperature is 1014 °C with maximum and minimum temperatures of 1063 °C and 987 °C in MOLB-type SOFC. In addition, it should be noted that the temperatures of PEN rise rapidly, reaching a maximum near the fuel inlet, and then gradually drop in those two types of SOFCs. This is due to offsetting effects of air near the inlet, at its coolest, being aligned with the fuel inlet. Of the two types of SOFCs, the MOLB-type SOFC has the higher average temperature and lower temperature difference (ΔT) than that of planar SOFC, which is similar to the co-flow case. Furthermore, the hydrogen mass fraction for both types of SOFCs also decrease along the fuel flow direction, but the difference of hydrogen mass fraction in the fuel inlet and outlet

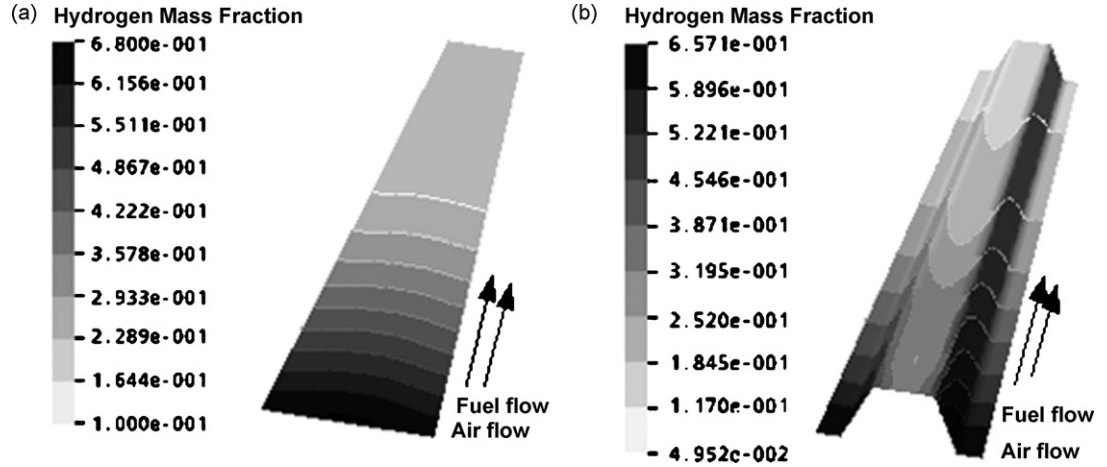

Fig. 3. Hydrogen mass fraction distributions on the interface between anode/electrolyte for the planar SOFC (a) and MOLB-type SOFC (b) in the co-flow case (no. 1).

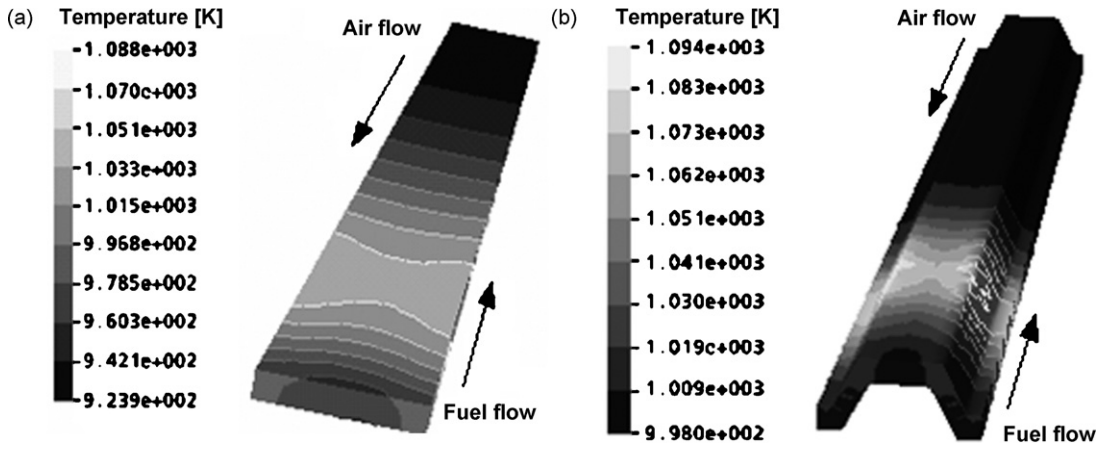

Fig. 4. PEN temperature distributions for planar SOFC (a) and MOLB-type SOFC (b) in the counter-flow case (no. 2).

is lower in MOLB-type SOFC (Fig. 5(b)) than that in planar SOFC (Fig. 5(a)), So more hydrogen is consumed because the hydrogen mass fraction in the fuel inlet is same, in other words, the fuel utilization is higher in the MOLB-type SOFC, which is similar to that in the co-flow case. However, the hydrogen mass fraction in the fuel outlet is higher in counter-flow case for two types of SOFCs, so the less hydrogen reacted and hydrogen utilizations are lower than those in co-flow case for the two types of SOFCs.

Consequently, overall considering the temperature distribution and the hydrogen utilization, it is advantage and suitable to choose the co-flow case for SOFCs steady operating.

For this flow case, the voltage is assumed constant and it is 0.3 V, several parameters influenced on the performances of two types of SOFCs are also compared. First, we focus on the effects of the fuel delivery rate on temperature distributions in those types of SOFCs. Fig. 6 shows the temperature distribution of the mid-plane in the *X*-direction for the co-flow case (no. 3). With the increase in the delivery rate of fuel, the average temperatures and temperature differences (ΔT) of PEN rise, which may cause larger thermal stress. This is because increment of the fuel delivery rate may cause the increasing of reaction rate, so more reaction heat was accumulated and the cell temperature rise.

Consistent with increasing of the hydrogen proportion from 80% to 90% and 100% in the fuel gas, the temperature differences and the average temperatures also rise due to the increase of reaction rate and more reaction heat accumulated, as shown in Fig. 7. Fig. 7 shows the temperature distribution of the mid-plane in the *X*-direction for the co-flow case (no. 4), although the general variation trends of temperatures are similar, the temperature of planar SOFC is more sensitive to the working conditions due to the less electrochemical reaction areas.

On the basis of the analysis on the temperature distributions mentioned above, in order to decrease the average temperatures and maximum temperatures, it is effective to increase delivery rate of air. In the SOFC system, air not only provides oxygen ions but also has the cooling function. Increasing the delivery rate of air, the average and maximum temperatures in those types of SOFCs drop, as shown in Fig. 8. This is because more reaction heat is absorbed and released by the air with the higher delivery rate, although the air utilizations are dropped.

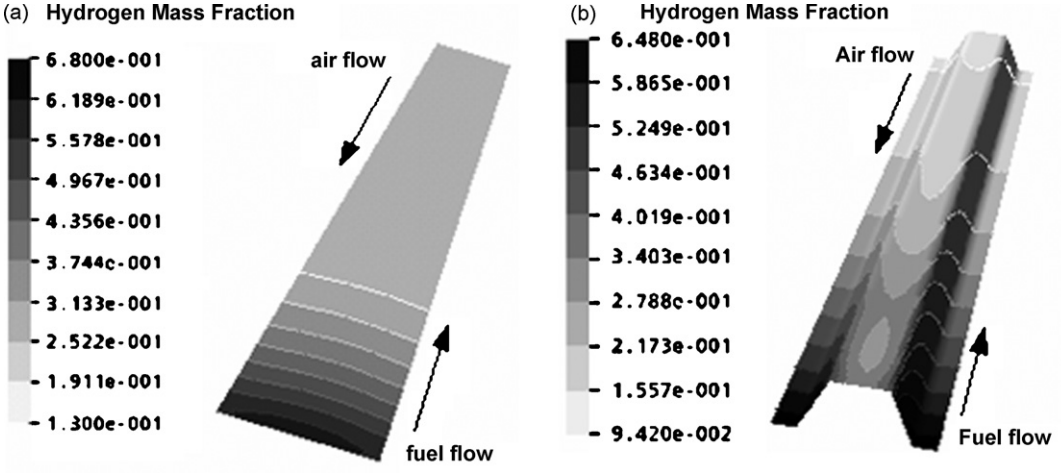

Fig. 5. Hydrogen mass fraction distributions on the interface between anode/electrolyte for the planar SOFC (a) and MOLB-type SOFC (b) in the counter-flow case (no. 2).

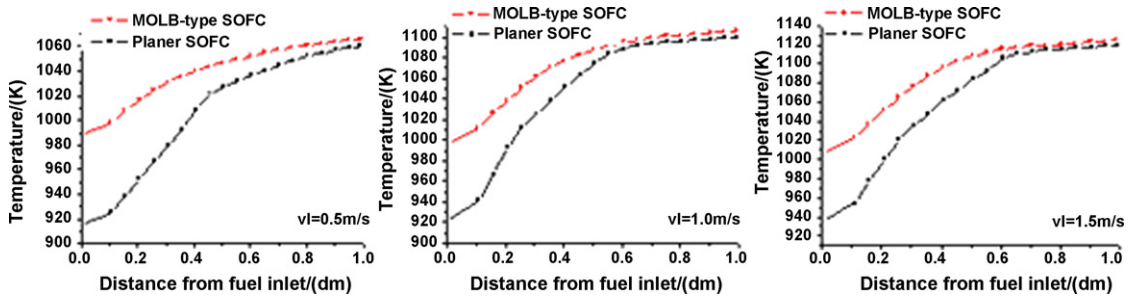

Fig. 6. Comparison of PEN temperature distributions between planar SOFC and MOLB-type SOFC in the co-flow case (no. 3).

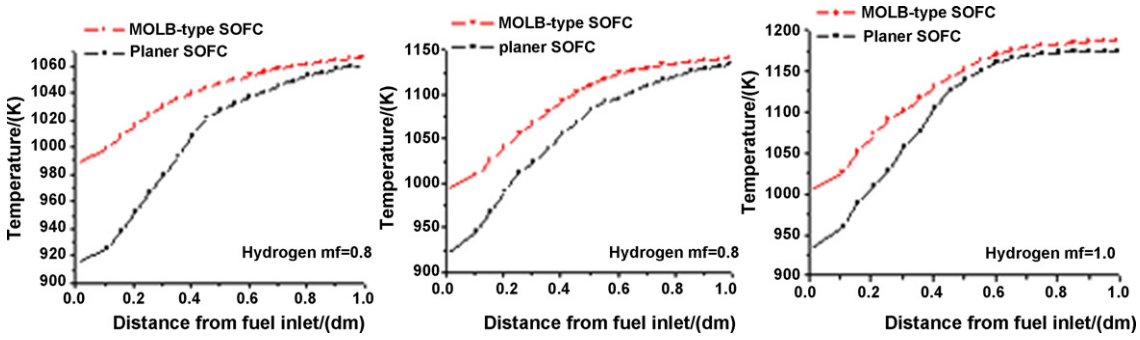

Fig. 7. Comparison of PEN temperature distributions between planar SOFC and MOLB-type SOFC in the co-flow case (no. 4).

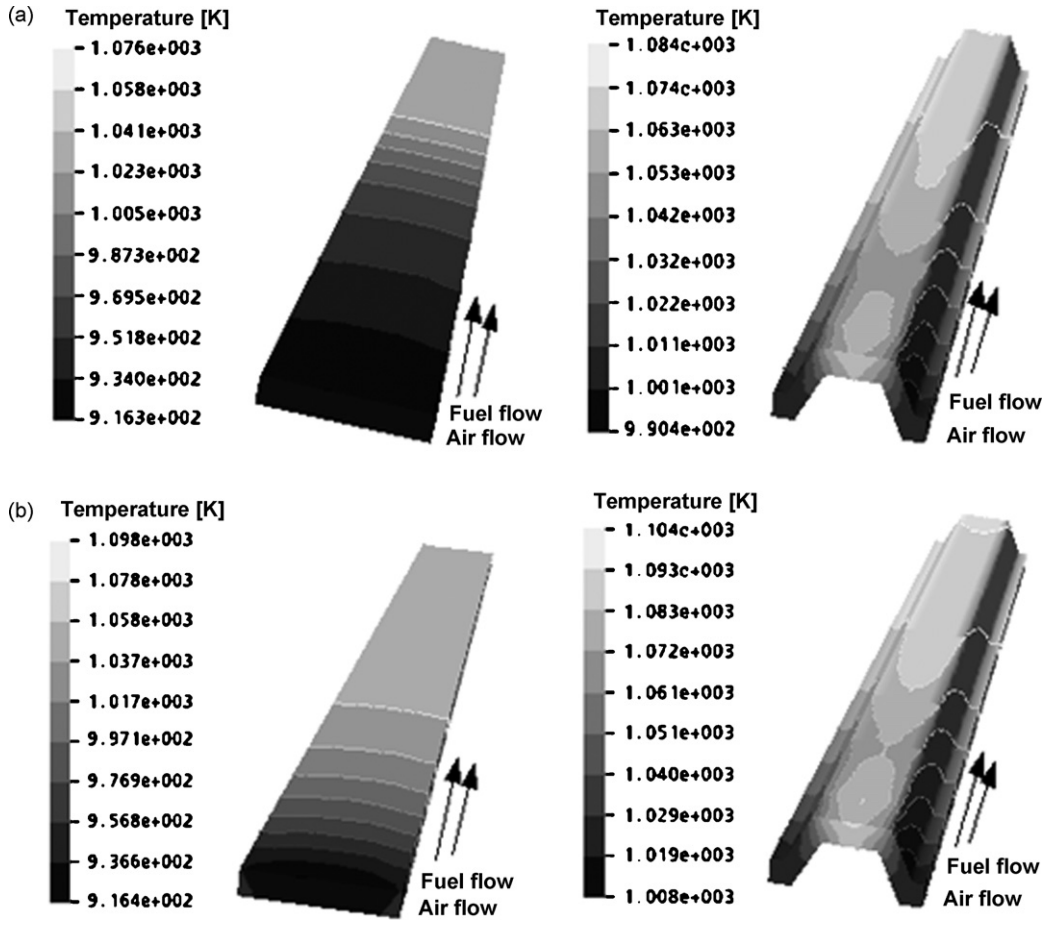

Fig. 8. Comparison of PEN temperature distributions between planar SOFC and MOLB-type SOFC in the co-flow case (no. 5).

5. Conclusions

The local current density was used to couple the thermo-fluid model with electrochemical model. The temperature distributions of planar and MOLB-type SOFCs in steady state were compared and some main conclusions were made as follows:

(1) In the co-flow case, the PEN temperature distributions in planar and MOLB-type SOFCs are more uniform than those in counter-flow case.
(2) Under the same work conditions, the temperature gradient is lower in MOLB-type SOFC than those in the planar SOFC.
(3) For co-flow case, under the constant voltage condition, with increasing the delivery rate of fuel gas or hydrogen mass fraction in the fuel, temperature gradients in the two types of SOFCs rise. Moreover, the temperature distributions in the planar SOFC are more sensitive to the variation of delivery rate of fuel and hydrogen mass fraction. In an attempt to achieve a more uniform temperature distribution, it is effective to decrease the temperature gradients of PEN by increasing the delivery rate of air.

Acknowledgements

The authors gratefully acknowledge the contribution of the National Nature Science Foundation of China (NSFC Nos. 50675081 and 50475134).

References

[1] S.C. Singhal, Solid State Ionics 135 (2000) 305–313.
[2] S.C. Singhal, Solid State Ionics 152/153 (2002) 405–410.
[3] B. Godfrey, K. Foger, R. Gillespie, R. Bolden, S.P.S. Badwal, J. Power Sources 86 (2002) 68–73.
[4] G.Y. Xie, K. Cui, J.Z. Xiao, X.L. Qian, J. Huazhong Univ. Sci. Technol. 30 (2002) 90–92 (in Chinese).
[5] H.W. Zheng, K.S. Ru, X.J. Zhang, J. Southwest China Normal Univ. 27 (2002) 789–793 (in Chinese).
[6] S.P. Simner, J.F. Bonnett, N.L. Canfield, K.D. Meinhardt, J.P. Shelton, V.L. Sprenkle, J.W. Stevenson, J. Power Sources 113 (2003) 1–10.
[7] T. Fukui, S. Ohara, M. Naito, K. Nogi, J. Power Sources 110 (2002) 91–95.
[8] S.P. Jiang, Y.Y. Duan, J.G. Love, J. Electrochem. Soc. 149 (2002) A1175–A1183.
[9] V.V. Kharton, E.V. Tsipis, A.A. Yaremchenko, J.R. Frade, Solid State Ionics 166 (2004) 327–337.
[10] T. Ishihara, S. Fukui, H. Nishiguchi, Y. Takita, J. Electrochem. Soc. 149 (2002) A823–A828.
[11] T. Hibino, A. Hashimoto, M. Suzuki, M. Yano, S. Yoshida, M. Sanob, J. Electrochem. Soc. 149 (2002) A195–A200.
[12] Z. Lin, J.W. Stevenson, M.A. Khaleel, J. Power Sources 117 (2003) 92–97.
[13] J.J. Hwang, C.K. Chen, D.Y. Lai, J. Power Sources 140 (2005) 235–242.
[14] M. Iwata, T. Hikosaka, M. Morita, T. Iwanari, K. Ito, K. Onda, Y. Eaaki, Y. Sakaki, S. Nagata, Solid State Ionics 132 (2000) 297–308.
[15] H. Yakabe, T. Ogiwara, M. Hishunuma, I. Yasuda, J. Power Sources 102 (2001) 144–154.
[16] H. Yakabe, T. Sakurai, Solid State Ionics 174 (2004) 295–302.
[17] H. Yakabe, Y. Baba, T. Sakurai, M. Satoh, I. Hirosawa, Y. Yoda, J. Power Sources 131 (2004) 278–284.
[18] K.P. Recknagle, R.E. Williford, L.A. Chick, D.R. Rector, M.A. Khaleel, J. Power Sources 113 (2003) 109–114.
[19] N. Autissier, D. Larrain, J. Van herle, D. Favrat, J. Power Sources 131 (2004) 313–319.
[20] Y. Shiratori, Y. Yamazaki, J. Power Sources 114 (2003) 80–87.
[21] J.J. Hwang, J. Fuel Cell Sci. Technol. 2 (2005) 164–170.
[22] J.J. Hwang, C.K. Chen, D.Y. Lai, J. Power Sources 143 (2005) 75–83.
[23] S.G. Neophytides, Chem. Eng. Sci. 54 (1999) 4603–4613.
[24] M. Iwata, T. Hikosaka, M. Morita, T. Iwanari, K. Ito, K. Onda, Y. Esaki, Y. Sakaki, S. Nagata, Solid State Ionics 132 (2000) 297–308.
[25] G.-T. Tang, Z.-Y. Luo, M.-J. Ni, C.-J. Yu, K.-F. Chen, Proceedings of the CSEE, vol. 25, 2005, pp. 116–121 (in Chinese).
[26] G. Wang, Y. Yang, H. Zhang, W. Xia, J. Power Sources, in press.
[27] J. Huang, Numerical Simulation of Heat and Mass Transfer in Solid Oxide Fuel Cell, Nanjing University of Science &Technology, 2004 (in Chinese).
[28] J.R. Ferguson, J.M. Fiard, R. Herbin, J. Power Sources 58 (2) (1996) 109–122.
[29] H. Yang, W. Lu, Applied Electrochemical, Scientific Publishing Center, Beijing, PR China, 2001 (in Chinese).
[30] S.H. Chan, K.A. Khor, Z.T. Xia, J. Power Sources (93) (2001) 130–140.